MAGNETIC RESONANCE IN CHEMISTRY
Magn. Reson. Chem. 2001; **39**: S18–S29

$^{1}H/^{15}N$ NMR chemical shielding, dipolar $^{15}N,^{2}H$ coupling and hydrogen bond geometry correlations in a novel series of hydrogen-bonded acid–base complexes of collidine with carboxylic acids

Phillipe Lorente,[1] Ilja G. Shenderovich,[1,2] Nikolai S. Golubev,[1,2] Gleb S. Denisov,[2] Gerd Buntkowsky[1] and Hans-Heinrich Limbach[1]*

[1] Institut für Chemie der Freien Universität Berlin, Takustrasse 3, D-14195, Berlin Germany
[2] Institute of Physics, St. Petersburg State University, 198504 St. Petersburg, Russia

Received 22 May 2001; Revised 23 August 2001; Accepted 24 August 2001

A novel series of hydrogen-bonded solid 1:1 acid–base complexes of ^{15}N-labeled 2,4,6-trimethylpyridine (collidine) with carboxylic acids and their hydrogen bond deuterated analogs were synthesized and studied by ^{1}H magic angle spinning (MAS) and ^{15}N cross-polarization NMR with and without MAS. Not only zwitterionic complexes with the H-bond proton closer to nitrogen than to oxygen but also molecular complexes have been observed, where the proton is located closer to oxygen. For these complexes, the isotropic ^{1}H and ^{15}N chemical shifts and the ^{15}N chemical shielding tensor elements were measured (the latter by lineshape simulation of the static powder spectra) as a function of the hydrogen bond geometry. For the deuterated analogs $^{1}H/^{2}H$ isotope effects on the isotropic ^{15}N chemical shifts were obtained under MAS conditions. Lineshape simulations of the static ^{15}N powder spectra revealed the dipolar $^{2}H,^{15}N$ couplings and hence the corresponding distances. The results reveal several hydrogen bond geometry–NMR parameter correlations which are analyzed in terms of the valence bond order model. (1) The collidine and apparently other pyridines isotropic ^{15}N chemical shifts depend in a characteristic way on the nitrogen–hydrogen distance. This correlation can be used in the future to evaluate hydrogen bond geometries and solid-state acidities in more complicated systems. (2) A correlation of the ^{1}H with the ^{15}N isotropic chemical shifts is observed which corresponds to the well-known hydrogen bond geometry correlation indicating a strong decrease of the A···B distance in an AHB hydrogen bond when the proton is shifted to the hydrogen bond center. This contraction is associated with a low-field ^{1}H NMR chemical shift. (3) The ^{15}N chemical shift anisotropy principal tensor elements δ_t, δ_r and $\delta_\perp$ (tangential, radial and perpendicular with respect to the pyridine ring) exhibit a linear relation with the isotropic ^{15}N chemical shifts. A crossing point of $\delta_t = \delta_r$ is observed. Further correlations of the hydrogen bond geometry with the geometric H/D isotope effects on the ^{15}N chemical shifts and with the pK_a values of the associated acids are reported.

KEYWORDS: NMR; ^{1}H NMR; ^{15}N NMR; collidine–carboxylic acid complexes; hydrogen bonding

INTRODUCTION

Whereas acid–base interactions in aqueous solutions can be described in terms of a conventional chemical equilibrium, the situation is very different in non-aqueous systems. Here, the acid and the base are in direct contact via a hydrogen bond. Such non-aqueous acid–base interactions between side-chains of amino acids play an important role in the structure and function of enzymes where bulk water is often absent in the active site.[1] In order to understand the influence of the variation of the relative acidity on the acid–base hydrogen bonds, some of us have carried out low-temperature NMR studies of hydrogen-bonded complexes of various bases such as pyridine,[2–4] 2,4,6-trimethylpyridine (collidine)[5,6] and other bases[6,7] with carboxylic and other acids. By using a polar Freon mixture, $CDF_2Cl–CDF_3$ (2:1), which is liquid down to 95 K we were able to characterize the intrinsic NMR parameters of a number of hydrogen-bonded complexes in the slow hydrogen bond exchange regime. Thus, as a function of the relative acidity of the components, the chemical shifts of the hydrogen-bonded protons and deuterons and also of the heavy atoms of the hydrogen

*Correspondence to: H.-H. Limbach, Institut für Chemie der Freien Universität Berlin, Takustrasse 3, D-14195, Berlin Germany.
Contract/grant sponsor: Deutsche Forschungsgeweinschaft.
Contract/grant sponsor: Fonds der Chemischen Industrie.
Contract/grant sponsor: German–Israel Foundation.
Contract/grant sponsor: Russian Foundation of Basic Research RFBR–DFG; Contract/grant number: 99-03-04026.

DOI: 10.1002/mrc.946

bridges such as ^{15}N or ^{19}F, or adjacent ^{13}C nuclei, could be measured which experience interesting H/D isotope[2,6] and temperature effects.[5] The phenomenon of scalar coupling between heavy atoms of the hydrogen bridges and of the proton across the hydrogen bonds was described,[7] in addition to H/D fractionation factors.[4] The main result of these studies is that an increase in the acidity of AH leads to a gradual transformation of the molecular hydrogen-bonded complex A—H···B via a proton-shared complex $A^{\delta-}\cdots H\cdots B^{\delta+}$ to a zwitterionic complex $A^-\cdots H—B^+$, where $A^{\delta-}\cdots H\cdots B^{\delta+}$ exhibits the shortest distance A···B and where the zwitterionic complexes are favored at low temperatures when the solvent polarity increases. During this transformation of the hydrogen bond O—H···N, the nitrogen signal experiences a monotonic upfield shift, whereas the proton resonates at the lowest field in the proton-shared complex $O^{\delta-}\cdots H\cdots N^{\delta+}$.

In order to exploit fully the power of liquid-state NMR in hydrogen bond research, it is desirable to establish direct links between hydrogen bond geometries, especially distances between hydrogen bond protons and their neighboring heavy atom nuclei and their NMR parameters. Because of the drawbacks of x-ray diffraction, solid-state NMR therefore plays an important role because (i) NMR parameters of hydrogen-bonded complexes $A^{\delta-}\cdots H\cdots B^{\delta+}$ are sensitive to the A···H and H···B distances, (ii) these distances can be obtained for NHN and OHN hydrogen bonds by dipolar $^1H-^{15}N$ NMR[8,9] and (iii) in combination with dipolar $^2H-^{15}N$ NMR it is possible to obtain very significant H/D isotope effects on these distances.[9,10] Unfortunately, the strong homonuclear ^1H dipolar couplings need to be decoupled in order to obtain the ^1H, ^{15}N dipolar couplings which are then scaled by a factor depending on the experimental setup which complicates the determination of H/D isotope effects on nitrogen–hydrogen distances. Another possibility is to deuterate overall the systems except the $^1H-^{15}N$ groups studied,[9,11] which is, however, not always possible.

Therefore, in the case of polycrystalline $[R—C\equiv N\cdots H\cdots N\equiv C—R]^-\ K^+$ salts and their deuterated analogs we used the following solid-state ^{15}N NMR approach.[10] First, using CP/MAS (CP = cross polarization, MAS = magic angle spinning), we determined the isotropic ^{15}N chemical shifts of the protonated and deuterated powdered salts, where we observed for the first time H/D isotope effects on solid-state NMR chemical shifts. Then, for the static powdered solids, we determined the values of the principal components of the nitrogen CSA tensor of the protonated hydrogen bond by ^{15}N lineshape analysis as a function of the hydrogen bond geometry. These tensor components were used to analyze the corresponding spectra of the deuterated salts and to determine the ^2H, ^{15}N dipolar coupling constants. As these constants are related to the distance between the coupled nuclei, nitrogen–deuteron distances could be measured as a function of the deuteron location and related to the isotropic nitrogen chemical shifts. The H/D isotope effects on the latter were then used to extrapolate the related nitrogen–hydrogen distances and hence the H/D isotope effects on the hydrogen bond geometries. These results were greatly assisted by *ab initio* calculations including corrections for anharmonic ground-state vibrations.

In this study, we combined both areas of research and describe here the results of solid-state NMR measurements of a series of novel solid-state acid–base 1 : 1 complexes between collidine and carboxylic acids depicted in Scheme 1. In this series the hydrogen bond proton is systematically shifted from oxygen to nitrogen. For the complexes **2**, **5** and **6** crystal structures at 150 K have been reported.[12] Two structures, those of **2** and **5**, are depicted in Fig. 1. Whereas **2** represents a typical molecular complex, exhibiting an N···O distance of 2.613(4) Å, there is evidence that **5** and **6** exhibit zwitterionic structures with N···O distances of 2.596(3) and 2.597(2) Å. One may even classify the latter as collidinium salts. We choose a pyridine derivative because of its heterocyclic nitrogen which represents a model for the proton acceptor nitrogen of the imidazole side-chain of histidine in proteins.

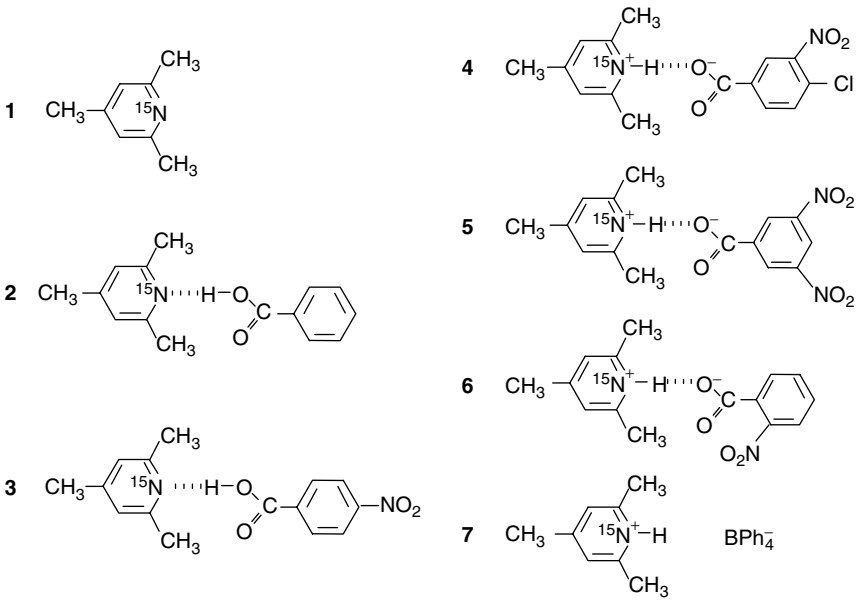

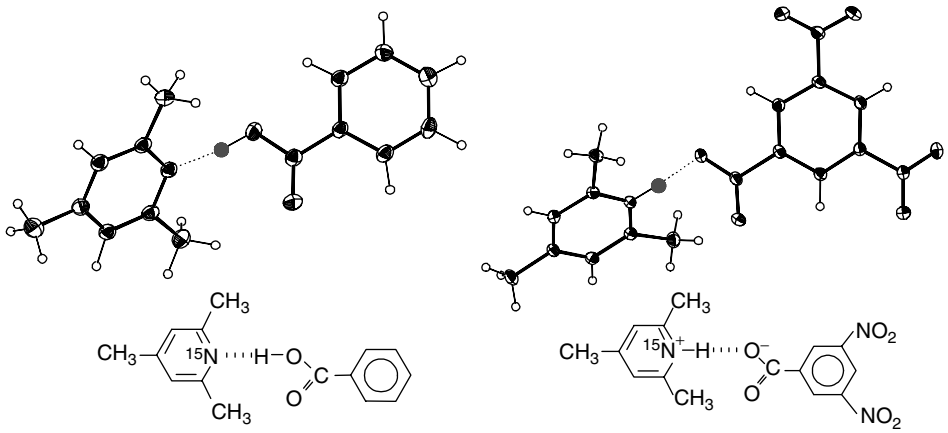

Figure 1. Crystallographic structures for the complexes **2** and **5** determined by x-ray diffraction at 150 K. Adapted from Foces-Foces *et al*.[12]

We chose collidine instead of pyridine whose ^{15}N chemical shielding tensor in the free compound and in pyridinium salts has been studied previously,[13] because in spite of many attempts we were not able to obtain solid 1 : 1 complexes of pyridine with the less acidic carboxylic acids such as benzoic acid where the competition between cyclic dimer and the 1 : 1 acid–base complex formation and the interplay with other intermolecular interactions apparently favors the former.

The scope of this paper is, therefore, to describe the results of our ^{15}N NMR studies and also additional ^{1}H NMR studies of this series of acid–base complexes. After the experimental section, which contains a description of the synthesis of the compounds, the details of the NMR measurements and the data analysis, the results are reported and discussed. One of the main results is a correlation between the nitrogen–hydrogen distances and both the ^{15}N and also ^{1}H chemical shifts of the NHO bonds as a function of the proton location. As in our previous studies,[4–6,7,10] we will make use of the valence bond order of hydrogen bonds[14] leading to a correlation of the two distances A···H and H···B of hydrogen-bonded complexes AHB.[15] In addition, we report H/D isotope effects on the ^{15}N NMR chemical shifts of the solid-state complexes **2**– **7**.

EXPERIMENTAL

Solid-state NMR measurements

Solid-state 9.12 MHz ^{15}N spectra were measured on a Bruker CXP 100 spectrometer (2.1 T) equipped with a Doty 7 mm CP/MAS probe at room temperature as described previously,[10] or a Bruker MSL 300 spectrometer (7 T) operating at 30.41 MHz for ^{15}N. ^{1}H MAS NMR spectra were measured on a Varian Infinity Plus 600 MHz solid-state NMR spectrometer. Standard $\{^{1}H\}$–^{15}N CP NMR experiments were performed under static or MAS conditions with continuous proton decoupling and an r.f. power of about 28 kHz. MAS spinning speeds were of the order of 2–3 kHz in the 9.12 MHz and 5–6 kHz in the 30.41 MHz experiments. The 90° pulse widths were about 6 μs, the CP contact times were between 2 and 8 ms and the recycle time was 3 s. All spectra are referenced to external solid $^{15}NH_4Cl$ (95% ^{15}N-enriched). In order to convert these data into the nitromethane scale, the relation

$$\delta(CH_3NO_2) = \delta(^{15}NH_4Cl_{cryst}) - 338.1\,\text{ppm}. \quad (1)$$

may be used.[16]

Materials

^{15}N-labeled 2,4,6-trimethylpyridine (collidine) (**1**) was synthesized from 95% ^{15}N-enriched NH_4Cl and 2,4,6- trimethylpyrylium tetrafluoroborate according to the method of Balaban *et al*.[17] Benzoic, 4-nitrobenzoic, 3-nitro-4-chlorobenzoic, 3,5-dinitrobenzoic, 2-nitrobenzoic, 3,5-dichlorobenzoic, 3,5-dinitro-4-methylbenzoic, 2-chloro-4-nitrobenzoic and hydrochloric acid and deuterium oxide, sodium tetraphenylborate and methanol-d_1 were purchased from Aldrich. The purity of the synthesized complexes was verified by ^{1}H NMR and ^{13}C NMR spectroscopy using chloroform solutions on a 270 MHz NMR spectrometer.

Compounds

[^{15}N]-2,4,6-Trimethylpyridine–benzoic acid (**2**), [^{15}N]-2,4,6-trimethylpyridine–4-nitrobenzoic acid (**3**), [^{15}N]-2,4,6-trimethylpyridine–4-chloro-3-nitrobenzoic acid (**4**), [^{15}N]-2,4,6-trimethylpyridine–3,5-dinitrobenzoic acid (**5**), [^{15}N]-2,4,6-trimethylpyridine–2-nitrobenzoic acid (**6**), [^{15}N]-2,4,6-trimethylpyridine–hydrochloric acid (**8**) and [^{15}N]-2,4,6-trimethylpyridine–2-chloro-4-nitrobenzoic acid (**9**) complexes were prepared using a solution in dichloromethane as an intermediate stage followed by azeotropic distillation. Microcrystalline powder was twice washed in diethyl ether to remove the excess of collidine. Finally, the complexes were recrystallized from diethyl ether at 253 K.

[^{15}N]-2,4,6-Trimethylpyridinium tetraphenylborate (**7**) was prepared from a 10% HCl solution of collidine after adding an excess of sodium tetraphenylborate. Since **7** is not soluble in water it was dried and recrystallized from acetone at 253 K.

Deuteration of these substances, performed by repeated distillation from methanol-d_1 solution, led to the corresponded samples **2D**, **3D**, **4D**, **5D** and **6D**. A sample of **7D** was specially prepared from DCl solution in deuterium oxide. The melting points of the polycrystalline samples were 339 (**2**), 408 (**3**), 355 (**4**), 423 (**5**), 361 (**6**), 373 (**9**) and >520 K (**7** and **8**).

As mentioned above, the x-ray crystal structures of **2**, **5** and **6** obtained at 150 K have been reported previously.[12] Unfortunately, we were not able to obtain crystals of the other complexes suitable for obtaining x-ray crystal structures. In addition to the problems of crystallization, crystalline **2** and **3** lost slowly collidine, especially during dehydration in a vacuum line, and were thereby converted into the

corresponding 1:2 complexes, as monitored by solid-state ^{15}N CP/MAS and ^{1}H MAS NMR.

Determination of N···H/N···D distances by dipolar ^{15}N solid-state NMR lineshape analysis

The ^{15}N NMR lineshape equations taking into account the heteronuclear dipolar coupling between the ^{15}N and a close deuteron have been described recently.[9] In this study, the same computer program was used and therefore it is not described further. All details concerning the means by which the couplings were obtained are given in the following section.

RESULTS

The results of the NMR experiments are depicted in Figs. 2–5. All parameters obtained are given in Table 1. The parameters are analyzed in Fig. 6 as described partly in this section and partly in the discussion section.

^{1}H MAS NMR measurements

In Fig. 2 are depicted the room-temperature ^{1}H MAS NMR spectra of the complexes **2**–**7** measured at a spinning speed of 24 kHz using a Varian Infinity Plus spectrometer operating at 600 MHz. As fast spinning removes homonuclear dipolar coupling to a large extent, we are able to observe the isotropic chemical shifts of the hydrogen-bonded complexes **2**–**6**. When the acidity of the carboxylic acid is increased, we observe in a similar way as for the complexes with pyridine in the liquid-state[3] first a low-field shift of the hydrogen bond

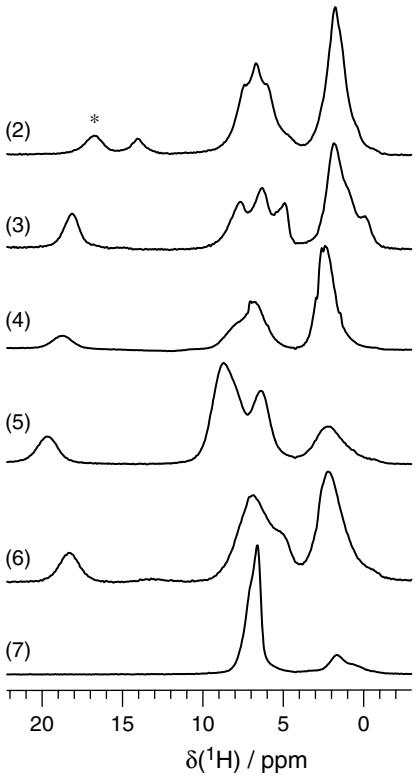

Figure 2. Room-temperature 600 MHz ^{1}H NMR spectra of compounds **2**–**7** at 24 kHz spinning speed. The spectra are referenced to external solid TMDS, $(CH_3)_3Si(CD_2)_2SO_3^-Na^+$. The asterisk indicates a 1:2 collidine–benzoic acid complex.

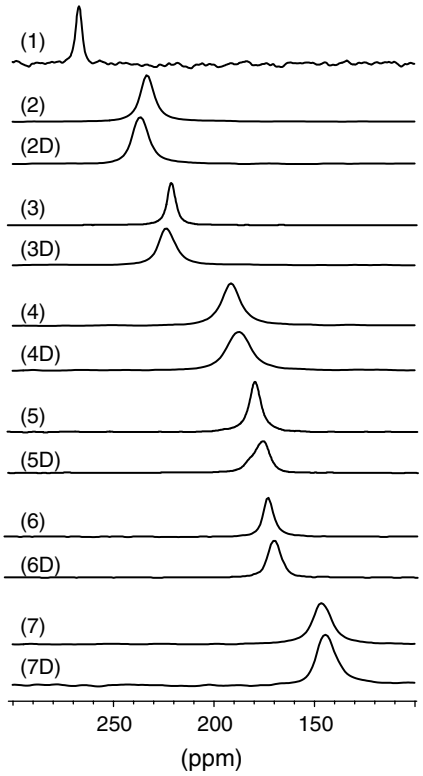

Figure 3. Room-temperature 9.12 MHz ^{15}N $\{^{1}H\}$ CP MAS NMR spectra of solid powder samples **2**–**7** and **2D**–**7D** at room temperature, 3 kHz spinning speed. The spectrum of **1** was obtained at 140 K. The spectra are referenced to external solid $^{15}NH_4Cl$.

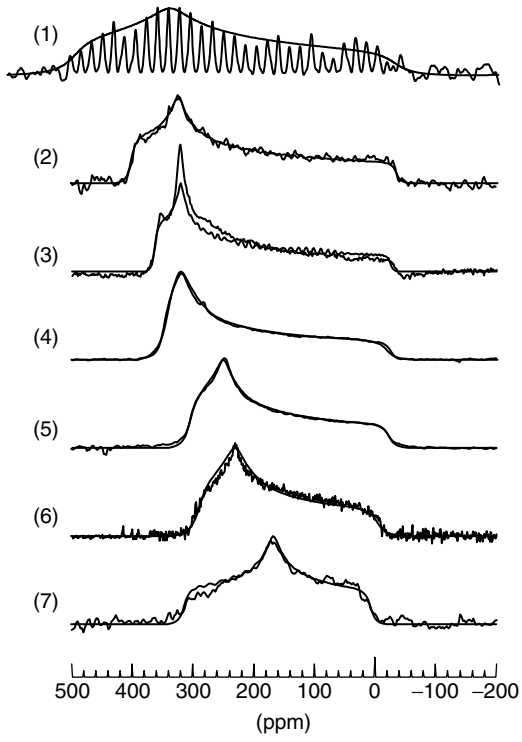

Figure 4. Superposed experimental and calculated 9.12 MHz ^{15}N $\{^{1}H\}$ CP NMR static spectra of solid powder samples **2**–**7** at room temperature. The spectrum of **1** was obtained at 30.41 MHz by slow MAS at 140 K with 540 Hz spinning speed. The spectra are referenced to external solid $^{15}NH_4Cl$.

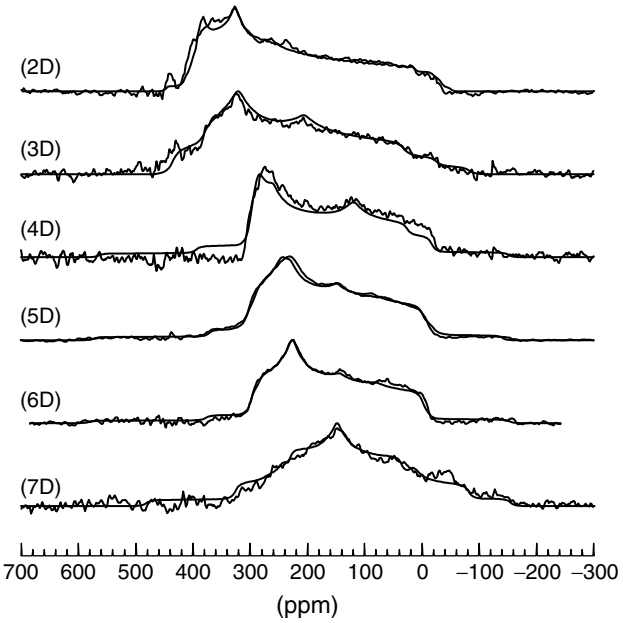

Figure 5. Superposed experimental and calculated 9.12 MHz ^{15}N $\{^1H\}$ CP NMR static spectra of deuterated solid powder samples **2D**–**7D** at room temperature. The spectra are referenced to external solid $^{15}NH_4Cl$.

proton to a maximum shift around 20 ppm and then again a high-field shift. Unfortunately, the hydrogen bond proton signal of **7** could not be identified. Either the chemical shift is around 10 ppm or smaller and hence hidden under the aromatic proton signals, or the signal is broadened owing to molecular motions interfering with MAS. Since the NH proton has no other protons in its direct vicinity, it experiences only comparably weak homonuclear dipolar interactions to other protons. Hence it should be possible either to observe this proton directly, employing ultra-fast MAS NMR spectroscopy and homonuclear dipolar decoupling, or indirectly via homonuclear dipolar decoupling and coherence transfer to the NH nitrogen.[18] Such experiments are currently under investigation.

^{15}N CP/MAS NMR measurements

The room-temperature 9.12 MHz ^{15}N CP/MAS NMR spectra of the ^{15}N-labeled compounds **2**–**7** and of their deuterated analogs **2D**–**7D** are depicted in Fig. 3. For comparison, the spectrum of neat frozen [^{15}N]collidine is also included. When the acidity of the carboxylic acid is increased, a monotonic shift of the [^{15}N]collidine signal to high-field is observed. Whereas deuteration causes a low-field shift of the signals for **2** and **3**, high-field shifts are observed for **5**–**7**, indicating opposite H/D isotope effects on the hydrogen bond geometries.

^{15}N CP NMR measurements of static powdered samples

The superimposed experimental and calculated room-temperature solid-state 9.12 MHz ^{15}N CP NMR spectra of the polycrystalline powders **2**–**7** are depicted in Fig. 4. The ^1H–^{15}N dipolar interaction is removed by the continuous proton decoupling. Hence the shape of the spectral lines depends only on the values of the chemical shift anisotropy (CSA) tensor components. The spectrum of frozen collidine collected at 140 K and 30.41 MHz was obtained using MAS at a low spinning speed of 540 Hz.

As a starting point, we made use of a similar analysis of [^{15}N]pyridine and [^{15}N]pyridinium reported by Solum *et al*.[13a] They found experimentally and by quantum mechanical calculations that the CSA tensors of pyridine and pyridinium are located in the molecular frame as indicated in Fig. 6. One of the principal CSA axes is the molecular symmetry axis, which is defined as the NC_4 axis, the second axis is the normal to the molecular plane and the third axis goes through atoms C-2 and C-6 (or C-3 and C-5). The corresponding principal chemical shielding values are labeled according to the literature for heterocyclic nitrogen atoms[13] as tangential component $\delta_{11} = \delta_t$, radial component $\delta_{22} = \delta_r$ and perpendicular component $\delta_{33} = \delta_\perp$. Solum *et al*.[13a] showed that for pyridine and pyridinium the values of δ_t and δ_r are inversed.

A more detailed view provides the present series of complexes for which a detailed analysis is depicted in Fig. 6(a), where we have plotted all components as a function of the isotropic ^{15}N chemical shifts. The latter is a sensitive gauge for the nitrogen–hydrogen distance, as shown later. For convenience and comparison in the future with other heterocyclic nitrogen atoms, we used neat frozen collidine as a reference, appearing at 268 ppm downfield of solid $^{15}NH_4Cl$ or at −70 ppm high field from liquid CH_3NO_2. We note that δ_r and $\delta_\perp$ are not very sensitive to the hydrogen bond geometry and move towards one another whereas δ_t is strongly shifted to high field when the proton approaches nitrogen. For **4**, δ_t and δ_r components are almost equal, leading to the appearance of a quasi-axial symmetric CSA tensor lineshape. The high-field shift of the isotropic value is, therefore, mainly determined by δ_t, so that a linear dependence of the tensor elements as a function of the isotropic chemical shifts has been observed. More details will be given in the discussion section.

At this stage, we were now able to analyze the corresponding room-temperature 9.12 MHz ^1H decoupled ^{15}N CP NMR static spectra of the powdered deuterated analogs **2D**–**7D** depicted in Fig. 5. These spectra are additionally affected by the dipolar ^2H–^{15}N interaction. The spectra were simulated by assuming that the N···D axis coincides with the NC_4 axis, i.e. parallel to δ_r. Thus, only the values of the dipolar coupling constants D^{ND} were varied, and no Euler angles relating the chemical shielding and the dipolar ND coupling tensors. The results of the coupling constants and the resulting cubic average distances r_{ND} are included in Table 1. The values of δ_t, δ_r and $\delta_\perp$ were not directly taken from the protonated compounds but extrapolated from Fig. 6(a) based on the isotropic ^{15}N chemical shifts of the deuterated compounds. The resulting calculated lineshapes in Fig. 5 are very satisfactory.

Finally, in Fig. 6(b) the cubic average distances r_{ND} obtained are plotted as a function of the isotropic nitrogen chemical shift. We obtained an exponential dependence. Again, the function represented by the dotted line will be given and discussed in the next section.

Table 1. Chemical shielding parameters of hydrogen-bonded acid–base complexes[a]

AHB	No.	M. P. (°C)	pK_a (AH)	$\delta(^1H)$ (ppm) (±0.1)	$\delta_{iso}(^{15}N)$ (ppm)[b] (±0.5)	$\delta_t(^{15}N)$ (ppm) (±3)	$\delta_r(^{15}N)$ (ppm) (±3)	$\delta_\perp(^{15}N)$ (ppm) (±3)	r_{NH}[c] (Å)	No.	$\delta_{iso}(^{15}N)$ (ppm) (±0.5)	$\delta_t(^{15}N)$ (ppm) (±5)	$\delta_r(^{15}N)$ (ppm) (±5)	$\delta_\perp(^{15}N)$ (ppm) (±5)	$^2\Delta^{15}N$ (D/H) (ppm) (±0.5)	D_{ND} (Hz)	r_{ND} (Å)
Col	**1**	—	—	—	0	222	67	−298	—						—		—
Bz–Col	**2**	66	4.19	14.0	−34	132	57	−293	1.60	**2D**	−31	142	58	−294	−3.2	410	1.64
																±15	±0.02
4-NO_2-Bz–Col	**3**	135	3.41	18.2	−47	102	52	−293	1.44	**3D**	−44	107	53	−293	−3.1	530	1.52
																±20	±0.00
4-Cl-3-NO_2-Bz–Col	**4**	78	3.66	18.9	−75	15	37	−283	1.23	**4D**	−81	0	34	−280	6.5	1250	1.14
																±50	±0.00
3,5-di-NO_2-Bz–Col	**5**	150	2.82	19.7	−89	−21	32	−278	1.16	**5D**	−93	−34	26	−273	4.0	1400	1.10
																±30	±0.02
2-NO_2-Bz–Col	**6**	88	2.16	18.3	−95	−40	22	−268	1.13	**6D**	−98	−50	22	−268	2.8	1400	1.10
																±100	±0.00
$HB(Ph)_4$–Col	**7**	>250	0		−120	−118	2	−248	1.02	**7D**	−122	−125	−1	−245	2.4	1600	1.06
																±100	±0.02
HCl–Col	**8**	>250	1	16.2	−105	—	—	—	1.08								
2-Cl-4-NO_2-Bz–Col	**9**	100	1.96		−81				1.20								
pyr	**10**		—		0	263[d]	96[d]	−359[d]									
HCl–pyr	**11**		1		−106[d]	308[d]	241[d]	−43[d]									

[a] Col = ^{15}N-labeled collidine; Bz = benzoic acid. δ_{iso} = isotropic ^{15}N chemical shifts obtained from the MAS spectra. δ_t, δ_r and $\delta_\perp$ = the principal components of the CSA tensor. $^2\Delta N(D/H)$ = H/D isotope effects on the ^{15}N isotropic chemical shifts. D = dipolar coupling constants. r_{ND} = cubic average distances N···D obtained by lineshape analysis.

[b] The ^{15}N chemical shifts of collidine and pyridine containing compounds are referenced to the corresponding free frozen bases, absorbing at 268 and 275 ppm (reference solid $^{15}NH_4Cl$) or −70 and −63 ppm (reference liquid nitromethane).

[c] Extrapolated using Eqn (13).

[d] Values according to Solum *et al.*[13]

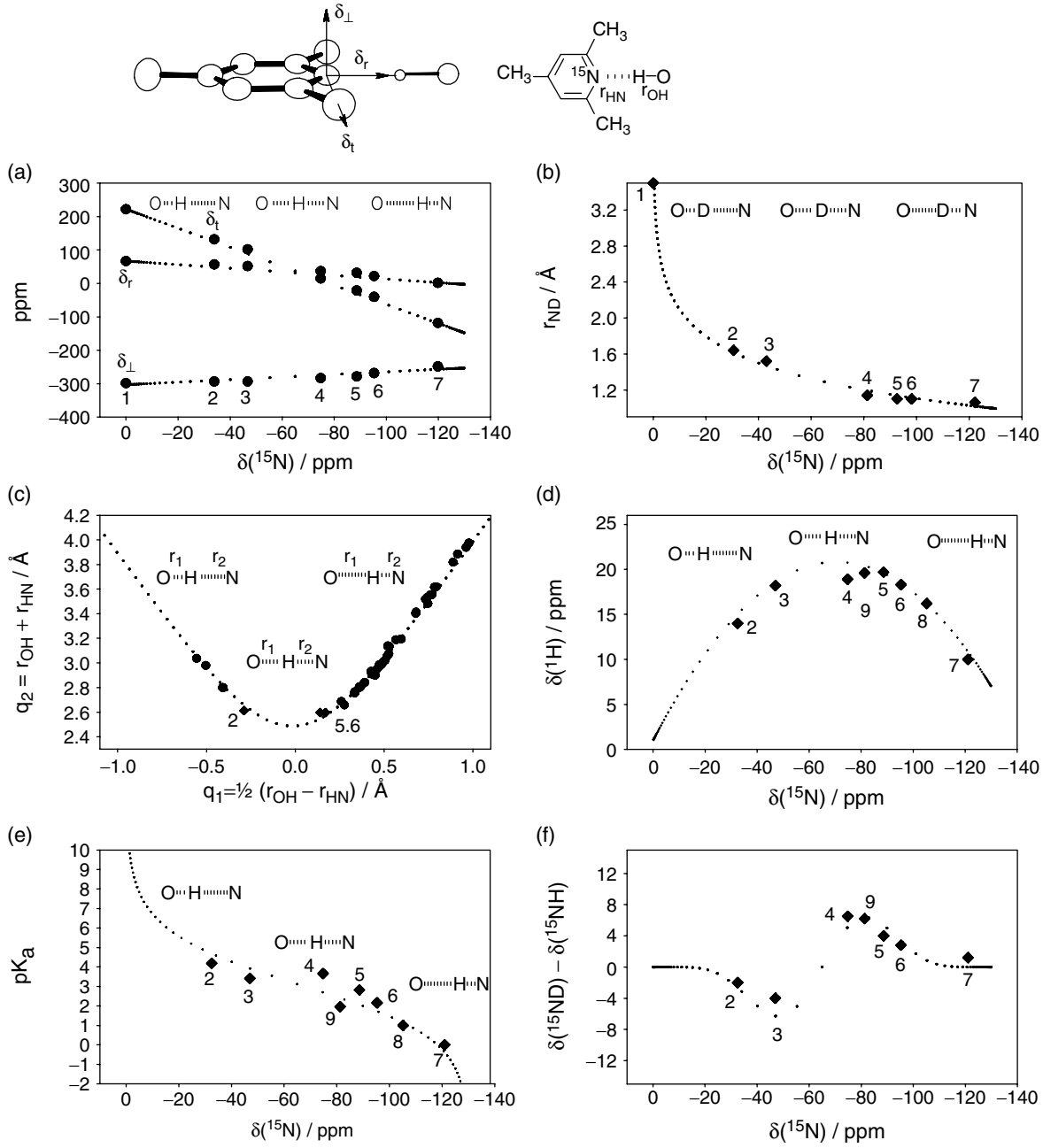

Figure 6. (a) Tangential component δ_t, radial component δ_r and perpendicular component $\delta_\perp$ of the [^{15}N]collidine CSA tensor as a function of the isotropic ^{15}N chemical shifts of the solid 1 : 1 collidine–acid complexes **2**–**7** and of neat frozen collidine **1**. (b) Cubic average distances r_{ND} obtained by ^{15}N CP NMR lineshape analysis of the deuterated analogs **2D**–**7D** as a function of their isotropic ^{15}N chemical shifts $\delta(^{15}N)$. (c) Hydrogen bond correlation $q_2 = r_{OH} + r_{HN}$ as a function of $q_1 = 1/2(r_{OH} - r_{HN})$ of NHO hydrogen-bonded solids. (●) Neutron data taken from Steiner;[15c] (♦) data for **2**, **5** and **6** obtained as described in the text. The dotted line was calculated using the parameters $r_{OH^\circ} = 0.942$ Å, $r_{HN^\circ} = 0.992$ Å, $b_{OH} = 0.371$ Å and $b_{HN} = 0.42$ Å as described in the text. (d) $\delta(^1H)$ vs $\delta(^{15}N)$ chemical shift correlation of the solids **2**–**9**. (e) pK_a values of the acid components of the solids **2**–**9** as a function of $\delta(^{15}N)$. (f) H/D isotope effect on the isotropic ^{15}N chemical shifts of **2**–**9** as a function of $\delta(^{15}N)$. For the calculation of the dotted lines, see text.

DISCUSSION

We have studied by solid-state ^{1}H and ^{15}N NMR the interaction of 2,4,6-trimethylpyridine (collidine) with various carboxylic acids in the solid-state. The series of compounds **2**–**7** allows us to follow the changes in the hydrogen bond geometries and of important NMR parameters when the proton is shifted from oxygen to nitrogen. In the following, we will analyze and discuss the results obtained. For this purpose, we will make extensive use of the valence bond order model of hydrogen bonding, reviewed briefly in the next section.

Valence bond order model of hydrogen bonding

One can associate with any hydrogen-bonded system A—H···B two distances $r_1 \equiv r_{AH}$ and $r_2 \equiv r_{HB}$ (using either

a bond labeling or an atom pair labeling) and an hydrogen bond angle ϑ as indicated in Scheme 2.

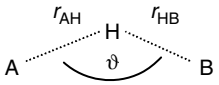

It is convenient to define additionally the coordinates q_1 and q_2 according to

$$q_1 = 1/2(r_{AH} - r_{HB})/2,\ q_2 = r_{AH} + r_{HB} \tag{2}$$

In the case of a linear hydrogen bond q_1 corresponds directly to the distance of the proton with respect to the hydrogen bond center and q_2 to the heavy atom A···B distance, as indicated in Scheme 3.

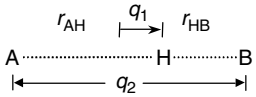

According to the valence bond order concept of Pauling and Brown,[14] one can define a valence p_{ij} of a diatomic molecule ij = AH as

$$p_{ij} = \exp[-(r_{ij} - r_{ij^\circ})/b_{ij}] \tag{3}$$

where b_{ij} is a decay parameter and r_{ij° the distance where $p_{ij} = 1$; p_{ij} becomes zero at infinite distance. A hydrogen-bonded system A—H···B is then characterized by two bond valences $p_1 = p_{AH}$ and $p_2 = p_{HB}$ and two distances $r_1 = r_{AH}$ and $r_2 = r_{HB}$ (Scheme 1). In this paper, A corresponds to oxygen and B to the nitrogen atom of collidine. The bond valence concept then assumes that the total bond order of hydrogen is unity:

$$\begin{aligned} 1 = p_{AH} + p_{HB} &= \exp[-(r_{AH} - r_{AH^\circ})/b_{AH}] \\ &\quad + \exp[-(r_{HB} - r_{HB^\circ})/b_{HB}] \\ &= \exp[-(q_1 + 1/2q_2 - r_{AH^\circ})/b_{AH}] \\ &\quad + \exp[-(-q_1 + 1/2q_2 - r_{HB^\circ})/b_{HB}] \end{aligned} \tag{4}$$

Hence, it follows that the two bond distances r_{AH} and r_{HB} or alternatively q_1 and q_2 cannot be varied independently. Whereas it is possible to express r_{AH} as a function of r_{HB}, the function of q_1 vs q_2 is calculated easily only numerically. Only in the cases of OHO or NHN hydrogen bonds where $b_{AH} = b_{HB} = b$ and $r_{AH^\circ} = r_{HB^\circ} = r^\circ$ does it follow from Eqn (4) that[10]

$$q_2 = r_{AH} + r_{HB} = 2r^\circ + 2q_1 + 2b\ln[1 + \exp(-2q_1/b)] \tag{5}$$

The validity of Eqn (4) has been demonstrated in the form of r_{AH} vs r_{HB} graphs by Steiner *et al.*[15] on the basis of a number of neutron diffraction structures contained in the Cambridge Structural Data Base. We have plotted the data points corresponding to OHN hydrogen bonds[15d] in the q_2 vs q_1 graph in Fig. 6(c). The calculated dotted curve indicates that when the proton is transferred from O to N the O···N distance first shortens, then reaches a minimum in the quasi-symmetric complex and finally widens again as the zwitterionic complex is approached. Unfortunately, data are lacking in the central region where the strongest hydrogen bonds are located. From this study, we included the data points for compounds **2**, **5** and **6**, derived by x-ray and NMR analyses as shown below. The dotted calculated curve was obtained as follows. For NHO bonds Steiner[15d] proposed the parameter set $r_{OH^\circ} = 0.942$ Å, $r_{HN^\circ} = 0.992$ Å, $b_{OH} = 0.371$ Å, $b_{HN} = 0.385$ Å. As already noted in the case of NHN bonds,[10b] these best-fit parameters depend somewhat on the body of data included in the fit. Especially the parameters b_{OH} and b_{HN} which determine the position of the minimum of the correlation curve depend somewhat on whether data points in the region of the minimum are included. By setting $b_{HN} = 0.42$ Å we obtain the calculated curve in Fig. 6(c) which differs from the curve calculated with the Steiner parameters only that the minimum is located at $q_{2\min} = 2.482$ Å and $q_{1\min} = -0.04$ Å whereas for $b_{HN} = 0.385$ Å we obtain $q_{2\min} = 2.458$ Å and $q_{1\min} = -0.03$ Å which can not be distinguished within the margin of error. Using the slightly higher value of b_{HN} we obtain, however, a better ^{1}H–^{15}N chemical shift correlation as described below.

In the following, we will use the hydrogen bond NMR parameters measured in terms of valence bond orders instead of distances. This procedure has the advantage that it reduces the number of parameters necessary to describe the dependence of these parameters on the hydrogen bond geometry.

^{15}N chemical shift–distance correlation

As we already proposed previously,[4] the isotropic ^{15}N chemical shifts of NHN and NHO hydrogen bonds depend to a good approximation in a linear way on the hydrogen–nitrogen bond order, i.e.

$$\begin{aligned} \delta(^{15}\mathrm{N}) = \delta &= \delta^\infty - (\delta^\infty - \delta^\circ)p_{HN},\ p_{HN} \\ &= \exp[-(r - r_{HN^\circ})/b_{HN}] \end{aligned} \tag{6}$$

As r_{HN° and b_{HN} are already given by the geometric H-bond correlation, only the two limiting nitrogen chemical shifts δ^∞ at infinite distance to the hydrogen bond proton and δ° at the distance r_{HN° need to be adapted. δ^∞ can be approximated from the pure base whereas δ° should be estimated independently. Both values depend on the type of base. As we have referenced all ^{15}N chemical shifts to bulk frozen solid collidine appearing at 268 ppm low-field from solid $^{15}NH_4Cl$ or −70 ppm high-field from liquid CH_3NO_2, we set $\delta^\infty = 0$. With respect to this reference, the value of $\delta^\infty - \delta^\circ = -\delta^\circ = 130$ ppm was then obtained by fitting the experimental ^{15}N chemical shifts of compounds **2D**–**7D** vs the dipolar distances r_{ND} using Eqn (6) as depicted in Fig. 6(b). The agreement between theory and experiment is very satisfactory. This equation will be helpful in the future as the nitrogen chemical shift of pyridine or collidine can now be directly converted into the N···H distance. It is remarkable that at the minimum N···O distance the

^{15}N chemical shift corresponds approximately to the value $(\delta^{\infty} - \delta^{\circ})/2$. Figure 6(c) illustrates why we chose to present the calculated curves of Fig. 6(b) and of Fig. 6(d)–6(f) as dotted lines: whereas the dots are equally spaced in Fig. 6(c), the corresponding dots in the other graphs are unequally spaced because they converge in the left and right limits. This is because NMR chemical shifts of the interacting partners AH and B have to become independent at longer distances. This convergence of the curves calculated by the valence bond order model is a great advantage over simple polynomials which are not restricted to a realistic range of chemical shift values. We note that the maximum spacing between the data dots corresponds to the minimum of the correlation curve of Fig. 6(c).

Encouraged by this result, we assumed a similar dependence as in Eqn (6) also for the three components δ_t, δ_r and $\delta_\perp$ of the ^{15}N tensor of collidine in the complexes. In other words, we assume a linear dependence of these quantities as a function of the corresponding isotropic chemical shifts given by

$$\delta_a(^{15}\mathrm{N}) = \delta_a = \delta_a^{\infty} + [(\delta_a^{\circ} - \delta_a^{\infty})/(\delta^{\circ} - \delta^{\infty})]\delta \qquad (7)$$

with $a = r, t, \perp$. With $\delta^{\infty} = 0$ we obtain $\delta_r^{\infty} = 222$ and $\delta_r^{\circ} = -148$ ppm, $\delta_t^{\infty} = 72$ and $\delta_r^{\circ} = 2$ ppm, and $\delta_\perp^{\infty} = -303$ and $\delta_\perp^{\circ} = -253$ ppm.

It is interesting that the crossing point of δ_t and δ_r occurs at the minimum of the correlation of Fig. 6(a) at the quasi-symmetric complex.

X-ray diffraction and NMR hydrogen bond distances

In Table 2 we compare the hydrogen bond geometries of the complexes **2**, **5** and **6** obtained by low-temperature x-ray crystallography[12] with those obtained by NMR.

First, we note that in addition to the experimental error of the dipolar coupling constants, the distances derived from these couplings are affected by a well-known systematic error, as the NMR distances represent average reversed cubic distances whereas neutron data represent mean distances. As we showed recently,[10] an anharmonic ground-state stretching vibration leads then to a slightly smaller cubic as compared with the mean average distance, although the effect is only of the order of a few percent. On the other hand, a large amplitude bending vibration or a libration of the N—D vector will increase the cubic average distance value obtained by dipolar NMR. Hence the distance values obtained here are uncorrected for vibrational and librational motions.

By contrast, a systematic error which would occur if one did not account for different geometries for the protonated and deuterated hydrogen bonds was eliminated by calculating the r_{NH} distances by extrapolation from the corresponding isotropic ^{15}N chemical shifts using Eqn (6). Assuming furthermore quasi-linear OHN hydrogen bonds, we can then calculate the r_{OH} distances as the difference $r_{OH} = r_{ON} - r_{NH}$ from the crystallographic r_{ON} distances (Table 2). Although the r_{NH} distances are in fact cubic averages and not mean average distances, and although the r_{OH} distances are calculated assuming quasi-linear hydrogen bonds, which is normally justified in the case of very strong hydrogen bonds, it is clear that these distances are closer to the truth than those derived from x-ray diffraction, where the values of r_{NH} obtained seem to be systematically shorter than those obtained by NMR, whereas the contrary is true for the values of r_{OH}. This interpretation is supported by the finding that the NMR-corrected data points for **2**, **5** and **6** are well located on the correlation line of Fig. 6(c), in contrast to the x-ray data.

^{1}H–^{15}N–chemical shift correlation

Recently, we also proposed the following correlation for the ^{1}H chemical shifts of pyridine–carboxylic acid complexes:[4]

$$\delta(^1\mathrm{H}) = \delta = 4\delta_H p_{OH} p_{HN} + \delta_{OH^\circ} p_{OH} + \delta_{HN^\circ} p_{HN} \qquad (8)$$

where δ_{OH° and δ_{HN° are the limiting ^{1}H chemical shifts of the isolated OH and NH groups. In addition to the linear terms in the OH and HN bond orders p_{OH} and p_{HN}, there is an excess term proportional to the product of the two bond orders. This product exhibits a maximum at $p_{OH} = p_{HN} = 0.5$. By combination of Eqns (6) and (8), taking into account Eqns (2)–(5) we were able to calculate the ^{1}H–^{15}N chemical shift correlation curve of Fig. 6(d), using the parameters $\delta_H = 16.7$ ppm, $\delta_{OH^\circ} = 1$ ppm and $\delta_{HN^\circ} = 7$ ppm. As we do not have enough data points in the wings of the curve, these parameters are preliminary and may be subject to small changes in the future. By comparison of Fig. 6(c) with Fig. 6(d), it becomes clear that the geometric hydrogen bond correlation transforms into chemical shifts which are then a measure of the former, with the feature that the chemical shift correlation is much more sensitive in the range of strong hydrogen bonds and less sensitive in the cases of weak hydrogen bonds, as compared with the geometric correlation.

Table 2. Comparison of x-ray and NMR crystallographic data

Complex	r_{NH}(Å)[a]	r_{OH}(Å)[a]	r_{ON}(Å)[a]	α(NHO)(°)[a]	r_{ND}(Å)[b]	r_{NH}(Å)[c]	r_{OH}(Å)[d]
Benzoic acid–coll. (**2**)	1.53	1.09	2.613	174	1.64	1.60	1.02
3,5-Dinitrobenzoic acid–coll. (**5**)	0.98	1.62	2.597	176	1.10	1.16	1.44
2-Nitrobenzoic acid–coll. (**6**)	0.94	1.65	2.596	171	1.10	1.13	1.47

[a] Ref. 12.

[b] ^{2}H–^{15}N dipolar NMR, this study.

[c] Extrapolated from the experimental ^{15}N chemical shifts using Eqn (12).

[d] $r_{OH} = r_{ON} - r_{NH}$.

pK_a–^{15}N chemical shift correlation

At this point we raise the question of the acid–base interaction in the solid-state. We have shown that an increase in the acidity of the acid interacting with collidine leads to geometric changes of the hydrogen bond from A—H···B via $A^{\delta-}\cdots H\cdots B^{\delta+}$ to $A^-\cdots H—B^+$, associated with a contraction of the A···B distance in $A^{\delta-}\cdots H\cdots B^{\delta+}$ responsible for the low-field ^{1}H chemical shift. Hence the situation is completely different to aqueous solution where the pK_a value of an acid is given by

$$HA(aq) + H_2O \rightleftharpoons A^-(aq) + H_3O^+(aq)$$
$$K_a^{AH} = (a_{H^+}a_{A^-})/a_{HA},\ pK_a^{AH} = -\log K_a^{AH} \qquad (9)$$

From a structural standpoint, both the solid-state hydrogen bond geometry and hence the intrinsic ^{15}N chemical shift of collidine hydrogen bonded to an acid as well as the pK_a value of the latter may have a similar origin. Therefore, it is tempting to look for a correlation between $\delta(^{15}N)$ and pK_a. Indeed, as depicted in Fig. 6(e), such a correlation seems to be fulfilled. For the calculation of this dependence we assumed a linear relation of pK_a with the proton transfer coordinate $q_1 = r_{OH} - r_{HN}$, given by

$$pK_a = -7q_1 + 2.8 \qquad (10)$$

The parameters of Eqn (10) were adapted in such a way that the calculated curve in Fig. 6(e) fits best the experimental data points. However, these parameters are only estimates in view of the scattering of the data.

Equation (10) indicates that in order to obtain a hydrogen bond with $q_1 = 0$, an acid with a pK_a value of ~3 is needed. As the pK_a value of collidinium is 7.43, this result means that this acid must be stronger than collidinium by about 4.5 units. A similar result has been obtained for solid 1 : 1 complexes of benzoic acids with pyridines by IR spectroscopy.[19]

Isotope effects on solid-state ^{15}N chemical shifts

Finally, we analyze the observed isotope effects on the ^{15}N chemical shifts. For this purpose, we assume that

$$p_{OH} + p_{NH} = p_{OD} + p_{ND} = 1 \qquad (11)$$

where p_{OH} and p_{OD} will be different for a given complex. We assume that the bond order changes after deuteration can be described in terms of a single parameter

$$\Delta p = 2(p_{ND} - p_{NH}) = -2(p_{OD} - p_{OH})$$
$$= p_{OH} - p_{OD} - (p_{NH} - p_{ND}) \qquad (12)$$

Now we assume the following relation, only justified later by comparison with experimental data:

$$\Delta p = A(p_{OH}p_{NH})^B(p_{NH} - p_{OH}) \qquad (13)$$

where A and B are adjustable parameters. Equation (13) allows us to associate with each value of r_{OH} and r_{HN}, i.e. of q_1^H and q_2^H, corresponding values of r_{OD} and r_{DN}, i.e. of q_1^D and q_2^D, and hence permits the calculation of ^{15}N and ^{2}H chemical shifts of the corresponding deuterated complexes using Eqns (6) and (7). Using the parameters $A = 10^4$ and $B = 7$ we obtain the graph of Fig. 6(f). There is a fairly good agreement between the experimental and calculated data.

The general shape of the calculated curve can be visualized as shown in Fig. 7, which displays the one-dimensional hydron potentials of AHB hydrogen bonds at fixed A···B distances. When the proton moves to the H-bond center, a contraction of the A···B distance results, in agreement with Fig. 6(c). After the proton has crossed the hydrogen bond center, an increase in the A···B distance results again. In the extreme situations where a proton is located preferentially on the heavy atom A or on B according to an asymmetric single well potential, substitution of H by D leads to a shortening of the shorter and a lengthening of the longer heavy atom–hydron bond. When A and B are equivalent, and the A···B distance is very short, there can be two different situations: if a system can adopt the shortest possible distance there will be a symmetric single well potential (right side) for the proton motion, otherwise a symmetric double well potential (left side) for the proton motion. The two situations are often difficult to distinguish. However, in the double well case the deuterons are always located closer to the heavy atoms than the proton leading

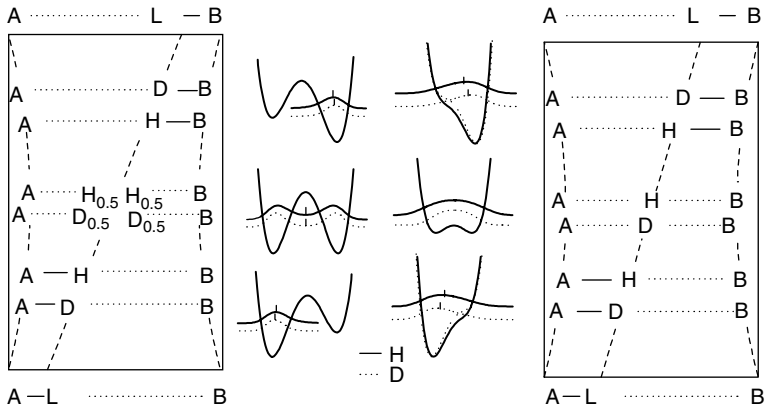

Figure 7. One-dimensional hydron (L = H, D) potentials and geometric changes during the transfer of a hydron from A to B characterized by the reaction coordinate $<r_1 - r_2>$. The squares of the wavefunctions of the vibrational groundstates for H and D, i.e. the proton and deuteron distribution functions, are included; however, for the sake of clarity, the difference in the one-dimensional potential functions for H and D according to Fig. 2 is omitted. (a) A barrier at the quasi-symmetric midpoint leads to a small H/D isotope effect on the geometry absent in case (b) with a very low barrier. Adapted from Smirnov *et al*.[2b]

always to an increased A···B distance upon deuteration, the deuteron is more confined in the hydrogen bond center in the single well case, as compared with the proton. This can also lead to a slight contraction of the A···B distance. From Fig. 7, it is also clear that the hydron zero-point energies (ZPE) will drop at the quasi-symmetric midpoint. The calculated ZPE values could also be expressed in terms of the valence bond order model.

CONCLUSIONS AND OUTLOOK

We have described a series of hydrogen-bonded solid 1 : 1 acid–base complexes of ^{15}N-labeled 2,4,6-trimethylpyridine (collidine) with carboxylic acids and their hydrogen bond deuterated analogs. In this series, a proton is systematically shifted from oxygen to nitrogen. During this process, the oxygen–nitrogen distance shortens when the proton is located in the hydrogen bond center. Thus, each complex can provide a snapshot of the proton motion in NHO hydrogen-bonded systems. Using a combination of high-resolution and dipolar ^{1}H and ^{15}N NMR, the worlds of hydrogen bond geometries and NMR shielding can be linked together, as both are intimately correlated. The determination of geometric H/D isotope effects arising from anharmonic motions provides interesting data to obtain the proton potential curves in the future. The results can be used in the future to determine hydrogen bond geometries of acid–base complexes of pyridine-type compounds from isotropic chemical shifts.

Let us finally comment on the method of determining ^{2}H-^{15}N dipolar couplings. Whereas in this and in our previous studies[9–11] we used the technique of lineshape analysis in order to determine these couplings, in view of the simplicity of our ^{15}N spectra, these couplings can no longer be easily obtained in this way in more complex systems. Therefore, Sack *et al*.[20] and Gullion[21] proposed REDOR-type techniques such as CPL-REDOR in order to obtain these couplings under MAS conditions, and Schmidt-Rohr and co-workers the RIDER technique.[22] All these sophisticated techniques measure the frequencies corresponding to the strength of the dipolar coupling indirectly from the dephasing of the signal of the X-nucleus, using composite pulses for inversion of the magnetization of the very broad ^{2}H signal. Since these techniques rely on the difference between the signal intensities of two separate experiments, a very good signal-to-noise ratio is necessary to calculate the distance information from the dephasing. Note also other improved two-dimensional rotational side-band techniques to measure ^{1}H–^{15}N dipolar couplings.[23]

On the other hand, the stratagem proposed here is to establish carefully distance–chemical shift correlations using the lineshape technique of model systems. For related systems the corresponding correlations can then be obtained in a simple way once the limiting shifts have been established. The distance information is encoded directly in the isotropic ^{15}N chemical shifts, which are much easier than the line intensities to determine accurately. In particular, one can hope that the correlation technique may be applicable to the nitrogen atoms of histidine in proteins and in mesoporous systems, because, together with the correlation, the ^{15}N CP/MAS spectrum corresponds directly to the nitrogen–hydrogen distance distribution function. An example of the application in this area will be published elsewhere (I. Shenderovich, P. Lorente, E. Gedat, G. Buntkowsky, A. Schreiber, G. Findenegg, N. S. Golubev and H.-H. Limbach, in preparation).

Acknowledgments

This work was supported by the Deutsche Forschungsgemeinschaft, Bonn-Bad Godesberg, the Fonds der Chemischen Industrie, Frankfurt, the German–Israel Foundation and the Russian Foundation of Basic Research RFBR–DFG grant 99-03-04026.

REFERENCES

1. (a) Cleland WW, Kreevoy MM. *Science* 1994; **264**: 1887; (b) Schowen KB, Schowen RL. *Methods Enzymol.* 1982; **87**: 551; (c) Gerlt JA, Kreevoy MM, Cleland WW, Frey PA. *Chem. Biol.* 1997; **4**: 259.
2. (a) Golubev NS, Smirnov SN, Gindin VA, Denisov GS, Benedict H, Limbach H-H. *J. Am. Chem. Soc.* 1994; **116**: 12 055; (b) Smirnov SN, Golubev NS, Denisov GS, Benedict H, Schah-Mohammedi P, Limbach H-H. *J. Am. Chem. Soc.* 1996; **118**: 4094.
3. Golubev NS, Denisov GS, Smirnov SN, Shchepkin DN, Limbach H-H. *Z. Phys. Chem.* 1996; **196**: 73.
4. Smirnov SN, Benedict H, Golubev NS, Denisov GS, Kreevoy MM, Schowen RL, Limbach H-H. *Can. J. Chem.* 1999; **77**: 943.
5. Golubev NS, Shenderovich IG, Smirnov SN, Denisov GS, Limbach H-H. *Chem. Eur. J.* 1999; **5**: 492.
6. Schah-Mohammedi P, Shenderovich IG, Detering C, Limbach H-H, Tolstoy PM, Smirnov SN, Denisov GS, Golubev NS. *J. Am. Chem. Soc.* 2000; **122**: 12 878.
7. (a) Shenderovich IG, Smirnov SN, Denisov GS, Gindin VA, Golubev NS, Dunger A, Reibke R, Kirpekar S, Malkina OL, Limbach H-H. *Ber. Bunsenges. Phys. Chem.* 1998; **102**: 422; (b) Benedict H, Shenderovich IG, Malkina OL, Malkin VG, Denisov GS, Golubev NS, Limbach H-H. *J. Am. Chem. Soc.* 2000; **122**: 1979.
8. (a) Stoll ME, Vega AJ, Vaughan RW. *J. Chem. Phys.* 1976; **65**: 4093; (b) Roberts JE, Harbison GS, Munowitz MG, Herzfeld J, Griffin RG. *J. Am. Chem. Soc.* 1987; **109**: 4163; (c) Tekely P, Montigny F, Canet D, Delpuech JJ. *Chem. Phys. Lett.* 1990; **175**: 401; (d) Munowitz MG, Griffin RG. *J. Chem. Phys.* 1982; **76**: 2848; (e) Munowitz MG, Aue WP, Griffin RG. *J. Chem. Phys.* 1982; **77**: 1686.
9. Hoelger CG, Limbach H-H. *J. Phys. Chem.* 1994; **98**: 11 803.
10. (a) Benedict H, Hoelger C, Aguilar-Parrilla F, Fehlhammer WP, Wehlan M, Janoschek R, Limbach H-H. *J. Mol. Struct.* 1996; **378**: 11; (b) Benedict H, Limbach HH, Wehlan M, Fehlhammer WP, Golubev NS, Janoschek R. *J. Am. Chem. Soc.* 1998; **120**: 2939.
11. Sack I, Macholl S, Wehrmann F, Albrecht J, Limbach HH, Fillaux F, Baron MH, Buntkowsky G. *Appl. Magn. Reson.* 2000; **17**: 413.
12. Foces-Foces C, Llamas-Saiz AL, Lorente P, Golubev NS, Limbach H-H. *Acta Crystallogr. Sect. C* 1999; **55**: 377.
13. (a) Solum MS, Altmann KL, Strohmeier M, Berges DA, Zhang Y, Facelli JC, Pugmire RJ, Grant DM. *J. Am. Chem. Soc.* 1997; **119**: 9804; (b) Schweitzer D, Spiess HW. *J. Magn. Reson.* 1974; **15**: 529; (c) Schurko RW, Wasylishen RE. *J. Phys. Chem. A* 2000; **104**: 3410.
14. (a) Pauling L. *J. Am. Chem. Soc.* 1947; **69**: 542; (b) Brown ID. *Acta Crystallogr. Sect. B* 1992; **48**: 553.
15. (a) Gilli P, Bertolasi V, Ferretti V, Gilli G. *J. Am. Chem. Soc.* 1994; **116**: 909; (b) Steiner Th, Saenger W. *Acta Crystallogr., Sect. B* 1994; **50**: 348; (c) Steiner Th. *J. Chem. Soc. Chem. Commun.* 1995; 1331; (d) Steiner Th. *J. Phys. Chem. A.* 1998; **102**: 7041.
16. (a) Witanowski M, Stefaniak L, Szymanski S, Januszewski H. *J. Magn. Reson.* 1977; **28**: 217; (b) Witanowski M, Stefaniak L, Webb GA. *Ann. Rep. NMR Spectrosc.* 1981; **11B**: 2; (c) Martin G,

Martin ML, Gouesnard JP. In *NMR-Basic Principles and Progress. Vol. 18, ^{15}N NMR Spectroscopy*. Springer: Heidelberg, 1989; 1; (d) Srinivasan PR, Lichter RL. *J. Magn. Reson.* 1977; **28**: 227.

17. (a) Balaban AT, Boulton AJ, McMahan DG, Baumgarten GHE. *Org. Synth. Coll.* 1973; **5**: 1112; (b) Golubev NS, Smirnov SN, Schah-Mohammedi P, Shenderovich IG, Denisov GS, Gindin VA, Limbach H-H. *Russ. J. Gen. Chem.* 1997; **67**: 1082.
18. (a) Saalwächter K, Graf R, Spiess HW. *J. Magn. Reson.* 2001; **148**: 398; (b) Schnell I, Langer B, Söntjens SHM, van Genderen MHP, Sijbesma RP, Spiess HW. *J. Magn. Reson.* 2001; **150**: 57; (c) Goward GR, Schnell I, Brown SP, Spiess HW, Kim HD, Ishida H. *Magn. Reson. Chem.* 2001; **39**: S5–S17.
19. Johnson SL, Rumon KA. *J. Phys. Chem.* 1965; **69**: 74.
20. Sack I, Goldbourt A, Vega S, Buntkowsky G. *J. Magn. Reson.* 1999; **138**: 54.
21. Gullion T. *J. Magn. Reson.* 2000; **146**: 220.
22. (a) Sandström D, Hong M, Schmidt-Rohr K. *Chem. Phys. Lett.* 1999; **300**: 213; (b) Saalwaechter K, Schmidt-Rohr K. *J. Magn. Reson.* 2000; **145**: 161.
23. Song X, Rienstra C, McDermott AE. *Magn. Reson. Chem.* 2001; **39**: S30–S36.